Occurrence of concurrent ‘orthogonal’ polarization modes in the Liénard-Wiechert field of a rotating superluminal source

A. Schmidt[1], H. Ardavan[2], J. Fasel[1],
J. Singleton[1], A. Ardavan[3]

[1]*Los Alamos National Laboratory, Los Alamos, NM 87545, USA*

[2]*Institute of Astronomy, University of Cambridge, Cambridge CB3 0HA, UK*

[3]*Clarendon Laboratory, University of Oxford, Oxford OX1 3PU, UK*

Summary

Moving sources of the electromagnetic radiation whose speeds exceed the speed of light *in vacuo* have already been generated in the laboratory.[1–3] Such sources are necessarily extended: their superluminally moving distribution patterns are created by the coordinated motion of aggregates of subluminally moving particles.[4–6] The field of a sufficiently localized source of this type in the far zone, however, is expected to have many features in common with that of a point-like source. Here we evaluate the Liénard-Wiechert field of a rotating superluminal point source numerically and show that this radiation field has the following intrinsic characteristics:

1. It is sharply focused along a rigidly rotating spirl-shaped beam that embodies the cusp of the envelope of the emitted wave fronts.

2. It consists of either one or three concurrent polarization modes (depending on the relative positions of the observer and the cusp) that constitute contributions to the field from differing retarded times.

3. Two of the modes are comparable in strength at both edges of the signal and dominate over the third everywhere except in the middle of the pulse.

4. The position angles of each of its dominant modes, as well as that of the total field, swing across the beam by as much as 180°.

5. The position angles of its two dominant modes remain approximately orthogonal throughout their excursion across the beam.

Given the fundamental nature of the Liénard-Wiechert field, the coincidence of these characteristics with those of the radio emission that is received from pulsars is striking.

For a volume-distributed source, the intensity of this emission along the caustics constituting the spiraling radiation beam decays like $1/R$ instead of $1/R^2$ with the distance R from its source.[7,8] This non-spherical decay has been demonstrated experimentally.[2,9] In addition, the radiation described here is broadband.[10] Coupled with these facts, the above results support the superluminal model of pulsars.[7,11,12]

1. Source of the radiation: polarization currents with superluminally rotating distribution patterns

Magnetic dipole radiation, at the rotation frequency ω of the central neutron star, gives rise to polarization currents in the plasma surrounding the magnetized star whose distribution patterns likewise rotate with the frequency ω:

$$j_{r,\varphi,z}(r,\varphi,z,t) = j_{r,\varphi,z}(r,\varphi-\omega t,z),$$

where (r,φ,z) are the cylindrical polar coordinates based on the axis of rotation and $j_{r,\varphi,z}$ are the cylindrical components of the polarization current density $\mathbf{j}$ that flows in the magnetosphere.

The induced current $\mathbf{j}$, which itself acts as a source of electromagnetic radiation[5,6], has a rigidly rotating distribution pattern whose outer parts (in $r > c/\omega$) move with linear speeds exceeding the speed of light *in vacuo*, c. This is not incompatible with special relativity because the superluminally moving pattern is created by the coordinated motion of subluminally moving particles.

In the far zone, the field of a circularly moving charge q with the trajectory

$$\mathbf{x} = \mathbf{x}(t): \qquad r = \text{const.}, \quad \varphi = \omega t, \quad z = 0,$$

shares many characteristics with that of an extended but localized source whose distribution pattern rotates rigidly.

2. Liénard-Wiechert field of a rotating superluminal source

The field of this source at $(\mathbf{x}_P, t_P)$ is given by

$$\mathbf{E}(\mathbf{x}_P, t_P) = q\sum_{t_{\rm ret}}\Big[\frac{(1-|\dot{\mathbf{x}}|^2/c^2)\mathbf{u}}{|1-\hat{\mathbf{n}}\cdot\dot{\mathbf{x}}/c|^3R^2(t)}+\frac{\hat{\mathbf{n}}\times(\mathbf{u}\times\ddot{\mathbf{x}})}{c^2|1-\hat{\mathbf{n}}\cdot\dot{\mathbf{x}}/c|^3R(t)}\Big],$$

$$\mathbf{B} = \hat{\mathbf{n}}\times\mathbf{E}.$$

Here, $\mathbf{R}(t) \equiv \mathbf{x}_P - \mathbf{x}$, $\dot{\mathbf{x}} \equiv d\mathbf{x}/dt$, $\mathbf{u} \equiv \hat{\mathbf{n}} - \dot{\mathbf{x}}/c$, and the unit vector $\hat{\mathbf{n}} \equiv \mathbf{R}/R$ designates the radiation direction. The summation extends over all values of the retarded time, i.e. all solutions $t_{\rm ret} < t_P$ of

$$\begin{aligned} t_P &= t + R(t)/c \\ &= t + [{z_P}^2 + {r_P}^2 + r^2 - 2rr_P\cos(\varphi_P - \omega t)]^{1/2}/c \\ &= h(t). \end{aligned}$$

Figure 1 shows the three characterisitic forms of $h(t)$, depending on the position of the observer. The retarded times $t_{\rm ret}$ contributing to the field at time t_P are the intersections of a horizontal line with one of the h curves in Fig. 1. Observers for whom $h(t)$ has the form (a) in this figure receive contributions from *three* earlier instants of the emission time t when the the observation time t_P lies in the interval $t_{P_+} < t_P < t_{P_-}$.

3. Envelope of the emitted wave fronts and its cusp

The waves whose emission times lie at the stationary points of curves (a) and (b) in Fig. 1 interfere constructively to form a Čerenkov-like envelope comprising two sheets: the surfaces ϕ_+ and ϕ_- shown in Fig. 2. The two sheets meet tangentially in a *cusp curve*: a caustic formed by the waves whose emission times lie at an inflection point of curve (b) in Fig. 1. The cusp is tangential to the light cylinder (the surface on which $\hat{r} \equiv r\omega/c = 1$) at a point in the plane of the source's orbit; it spirals upward and outward (and symmetrically, downward and outward) from this point, approaching the double cone $\sin\theta_P = \hat{r}^{-1}$. Figure 3 shows this cusp curve, together with the light cylinder.

The envelope rotates rigidly with the angular frequency ω. A fixed observer receives a single wave front, and so sees a single image of the source, when s/he is outside the envelope. But as one of the sheets of this surface swings past the observer and s/he enters the envelope, s/he receives three wave fronts simultaneously, thus detecting three images of the source; see Fig. 4. The three contributing retarded times in the expression for the Liénard-Wiechert field correspond to the emission times of these three images.

4. Field strength

Most of the energy of the field is concentrated in the vicinities of the envelope and its cusp. These are the regions for which a sustained interval of retarded time contributes to an instant of observation time. For an extended source, the field strength along the cusp directions is proportional to ${R_P}^{-1/2}$, rather than ${R_P}^{-1}$.[7,8] This nonspherical decay boosts the brightness temperature of the source by a factor of the order of $R_P\omega/c$.[7,12].

Figure 5 is a plot of relative field strengths in the plane of source's orbit (cf. Fig. 2). Figure 6 is a similar field-strength plot on the cone that is the asymptote of the cusp spiral.

Because the field of the rotating source itself rotates rigidly, an observer at spherical coordinates $(R_P, \varphi_P, \theta_P)$ samples, during each rotation period, the field on the latitude line of polar angle θ_P of the sphere of radius R_P. Figure 7 shows the strengths of each of the three images (i.e. the contributions to the magnitude of the field from each of the three retarded times) for a small segment of such a latitude line near the cusp on a sphere of radius $R_P = 10^{10}c/\omega$. Note that the field is much stronger at the inner edge (as compared to that at the outer edge) of each sheet of the envelope, and that, within the envelope near the cusp, two of the contributing fields are stronger than the third on either side of the pulse center.

5. Polarization

Figure 8 shows the polarization position angles and the strength of the field outside the envelope where the contributions towards the field at any given observation point are made at only a single value of the retarded time, i.e. where there is only a single polarization mode.

Polarization position angles for observation points on the cone $\theta_P = \pi/4$ within the envelope are shown in Fig. 9. While the two modes that are shown, namely those due to wave fronts emitted at t_1 and t_3, are nearly orthogonal, the radiation emitted at t_2 serves as a modal connecting bridge joining the polarization position angle trajectories of the other two modes over much of the pulse, thereby following their rapid polarization-angle change.

Figure 10 shows the polarization-position angles for the three contributing retarded times corresponding to the same observational arc for which Fig. 7 shows field strengths. The envelope is modally connected by wave fronts emitted at t_2. Within the envelope near the cusp, two of the contributing fields are found to be stronger than the third on either side of the pulse center, with the first retarded time's contribution being weakest before the pulse center and the third, after. The average position angle swings rapidly around the pulse center by about 90°.

Figure 11 shows the polarization position angles of the total field on a sphere in the far zone. The longitudinal angle φ is here plotted along the abscissa, so that a fixed observer samples a vertical slice of the shown distribution. Note that in the vicinities of the two points at which the cusp of the envelope intersects the sphere the polarization position angle swings through 180°, whether observed inside or outside the envelope.

Figure 12 shows the position angles of the corresponding two ‘orthogonal’ polarization modes that are observable inside the envelope.

References

1. Bessarab, A. V., Gorbunov, A. A., Martynenko, S. P. & Prudkoy, N. A. Faster-than-light EMP source initiated by short X-ray pulse of laser plasma. IEEE Trans. on Plasma Sci. **32** (3), 1400–1404 (2004).

2. Ardavan, A., Hayes, W., Singleton, J., Ardavan, H., Fopma, J. & Halliday, D. Experimental observation of nonspherically-decaying radiation from a rotating superluminal source. J. Appl. Phys. **96**, 4614–4631 (2004); **96**, 7760–7777(E) (2004).

3. Bolotovskii, B. M. & Serov, A. V. Radiation of superluminal sources in vacuum. Uspekhi Fizicheskikh Nauk **175** (9), 943–955 (2005).

4. Bolotovskii, B. M. & Ginzburg, V. L. The Vavilov-Cerenkov effect and the Doppler effect in the motion of sources with superluminal velocity in vacuum. Sov. Phys. Usp. **15** (2), 184–192 (1972).

5. Ginzburg, V. L. Vavilov-Cerenkov effect and anomalous Doppler effect in a medium in which the wave phase velocity exceeds the speed of light in vacuum. Sov. Phys. JETP **35** (1), 92–93 (1972).

6. Bolotovskii, B. M. & Bykov, V. P. Radiation by charges moving faster than light. Sov. Phys. Usp. **33**, 477–487 (1990).

7. Ardavan, H. Generastion of focused, nonspherically decaying pulses of electromagnetic radiation. Phys. Rev. E **58** (8), 6659–6684 (1998).

8. Ardavan, H., Ardavan, A. & Singleton, J. Spectral and polarization characteristics of the nonspherically decaying radiation generated by polarization currents with superluminally rotating distribution patterns. J. Opt. Soc. Am. A **21** (5), 858–872 (2004).

9. Singleton, J., Ardavan, A., Ardavan, H., Fopma, J., Halliday, D. & Hayes, W. Experimental demonstration of emission from a superluminal polarization current—a new class of solid-state source for MHz-THz and beyond. IEEE Conference Digest **04EX857**, 591 (2004).

10. Ardavan, H., Ardavan, A. & Singleton, J. Frequency spectrum of focused broadband pulses of electromagnetic radiation generated by polarization currents with superluminally rotating distribution patterns. J. Opt. Soc. Am. A **20** (11), 2137–2155 (2003).

11. Ardavan, H. The mechanism of radiation in pulsars. Mon. Not. R. Astron. Soc **268**, 361–392 (1994).

12. Ardavan, H. The superluminal model of pulsars. in *Pulsar Astronomy—2000 and beyond, IAU Colloq. 177* (eds Kramer, M. Wex, N. & Wielebinski, R.) 365–366 (ASP Conf. Ser. Vol 202, Astronomical Society of the Pacific, San Francisco, 2000).

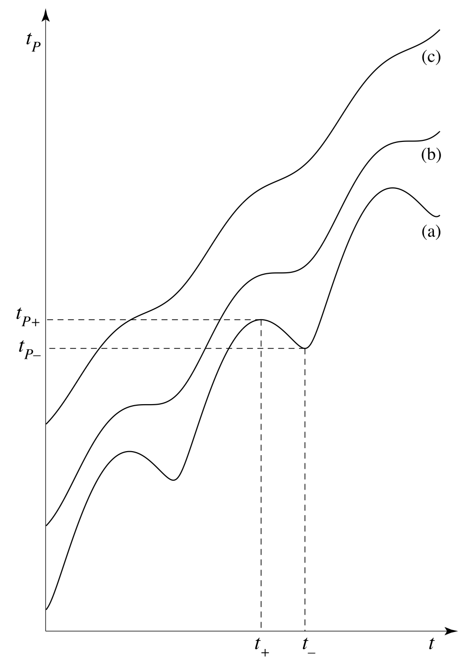

Figure 1: Observation time t_P versus the emission time t. Curves representing $h(t)$ for an observation point within or on (a), on the cusp of (b), and outside (c) the envelope. Curve (a) shows that the observation times between t_{P_-} and t_{P_+} correspond to three emission times.

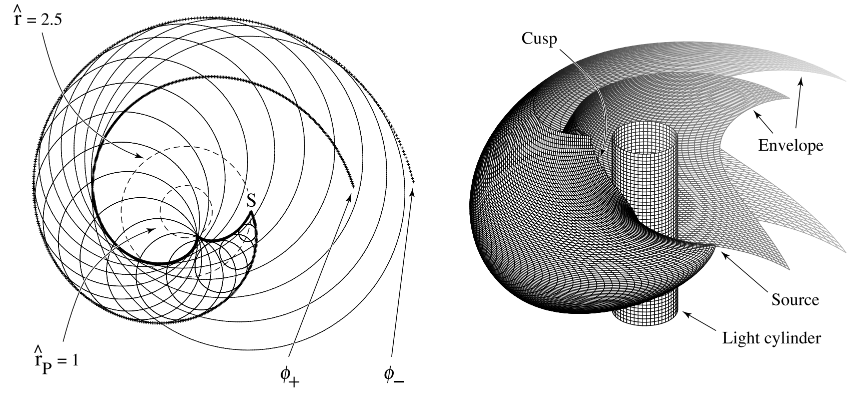

(a) (b)

Figure 2: The emitted Huygens wavelets and their envelope for a source S rotating with a constant angular velocity ω on a circle of radius $r = 2.5c/\omega$ (the outer dashed circle). (a) Cross sections of the wave fronts and their envelope with the plane of source's orbit. (b) The three-dimensional view of the light cylinder and the envelope for the same source S. The solid circles are the wavefronts emanating from the source. The bold curves designate the two sheets ϕ_+ and ϕ_- of the envelope. The cusp at which the two sheets of the envelope meet touches the light cylinder (the inner dashed circle) in the plane of rotation.

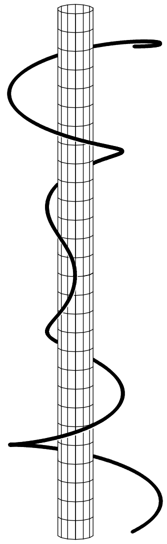

Figure 3: Cusp locus of the envelope. Segment $-15 \le \hat{z}_P \le 15$ of the cusp for $\hat{r} \equiv r\omega/c = 2.5$, together with the light cylinder. The curve is tangent to the light cylinder in the source's plane of rotation and spirals outward from there, approaching the double cone $\sin\theta_P = \hat{r}^{-1}$.

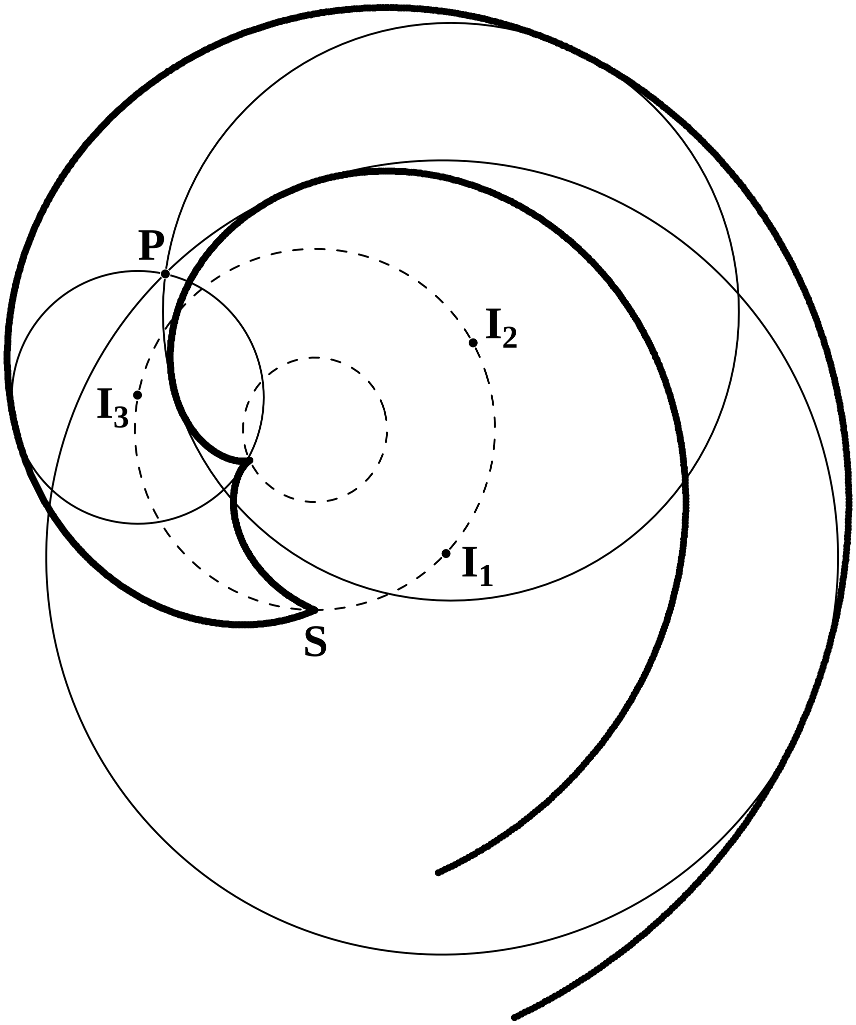

Figure 4: The three images of the source emitted at the three contributing retarded times. An observer P inside the envelope simultaneously receives three wave fronts each of which is emitted at a different retarded (emission) time. The corresponding retarded positions I_1, I_2 and I_3 of the source (the centers of the intersecting wave fronts) are observed as three distinct images of this source.[6] (Cf. Fig. 1.)

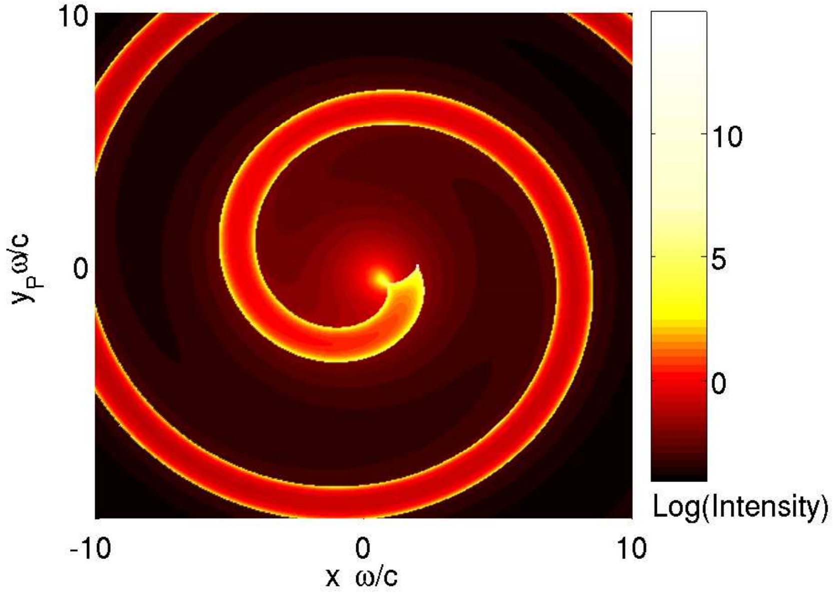

Figure 5: Field strength in the plane of rotation, for $\hat{r} \equiv r\omega/c = 2.5$. (Cf. Fig. 2.) Note the higher strength of the field along the inner edges of the envelope and near the cusp.

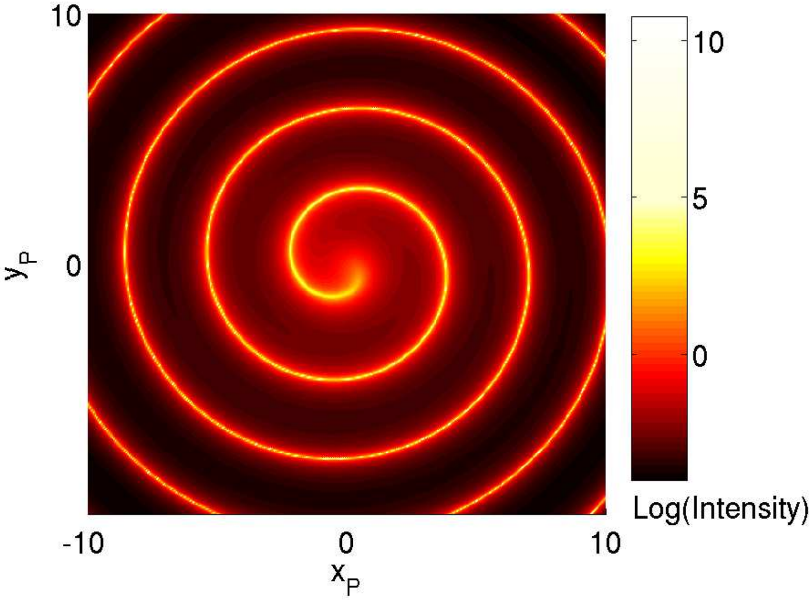

Figure 6: Field strength on the cusp, for $\hat{r} \equiv r\omega/c = 2.5$. The distribution of field strength on the cone $\theta_P = \arcsin \hat{r}^{-1}$ containing the cusp. The cusp rapidly approaches this cone over the first rotation of the spiral and extends all the way to infinity. (Cf. Fig. 3.)

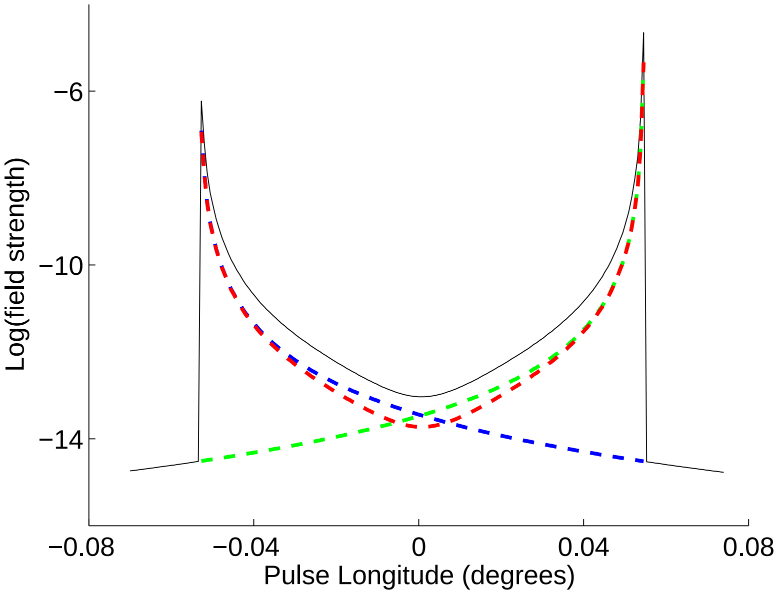

Figure 7: The relative strengths of the three distinct images of the source as observed near the cusp on a sphere of large radius. For a source with $\hat{r} \equiv r\omega/c = 1.1$, total field strength (black) and strengths of the underlying contributions from the three retarded times (green, red, blue) on a small arc of the circle $\hat{R}_P \equiv R_P\omega/c = 10^{10}$, $\theta_P = \pi/2.7$, crossing the envelope near the cusp. Note that the contribution from the third retarded time is much stronger than that of the first near the beginning of the pulse, with these rôles reversed near the end. Note also that two of the contributions are stronger than the third everywhere except in the middle of the pulse.

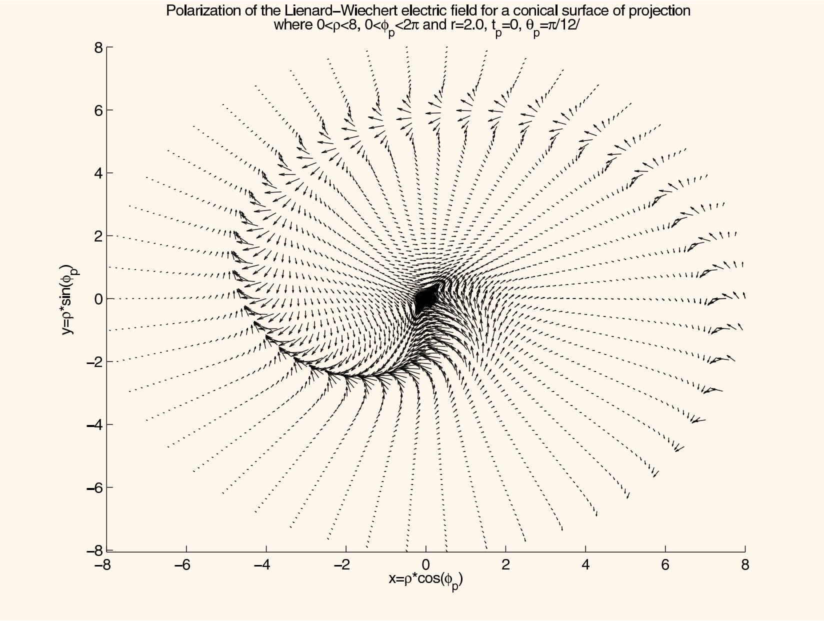

Figure 8: Polarization position angles and field strengths for a source with $r\omega = 2c$ on the cone $\theta_P = \pi/12$ outside the envelope.

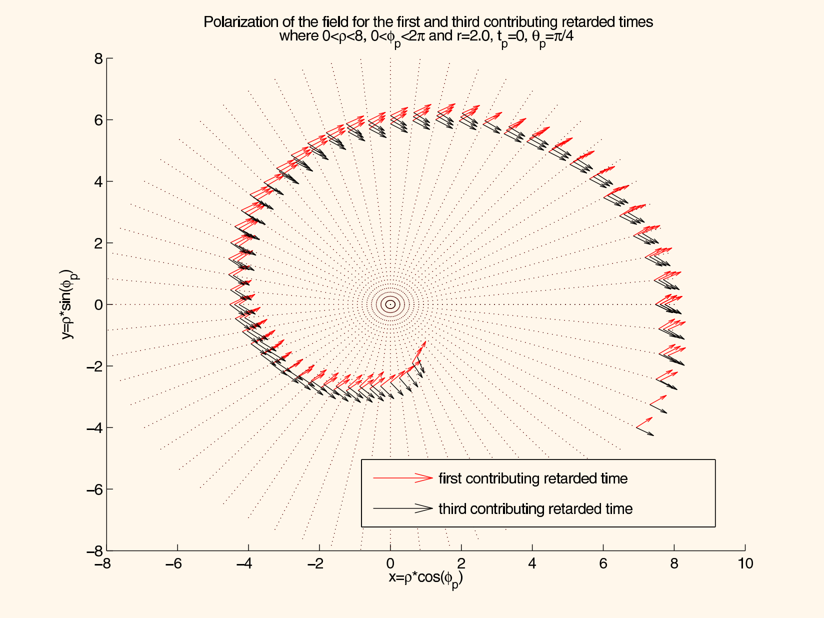

Figure 9: Polarization position angles of the two stronger images. The arrows represent the directions (but not the magnitudes) of the dominant two of the three simultaneously received contributions to the electric field for $r\omega = 2c$ on the cone $\theta_P = \pi/4$. These would be observed as concurrent polarization modes. Note that the position angles of these two modes are approximately orthogonal everywhere. (Cf. Fig. 10.)

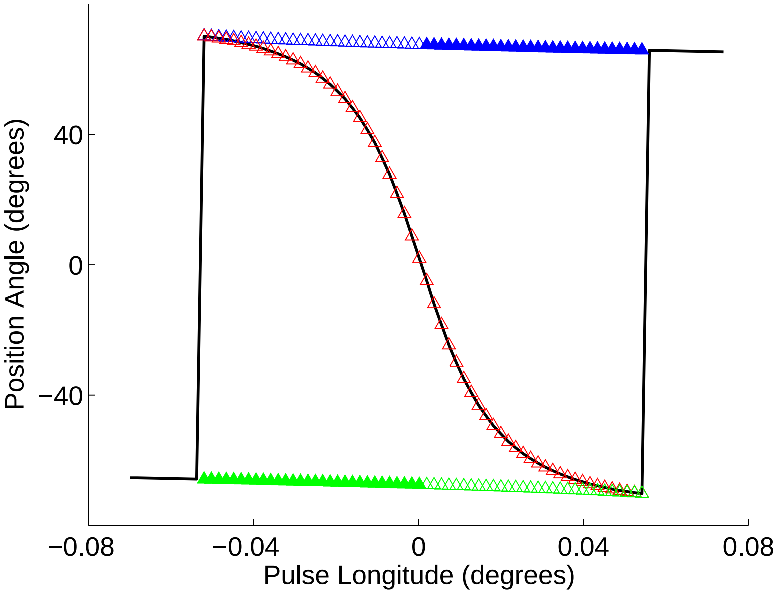

Figure 10: Position angles of the contributions from the three retarded times relative to one another and to that of the total field. For the same source and observation arc as in Figure (**??**), the position angles of the contributions from the three retarded times (green, red, and blue triangles) and the position angle of the total field (black line). The position angles of the dominant contributions are shown with open triangles, and those of the weakest contribution with filled triangles. Note that the the first and third contributions remain approximately orthogonal across the pulse and that the position angle of the second contribution closely follows the average position angle, bridging the first and third contributions.

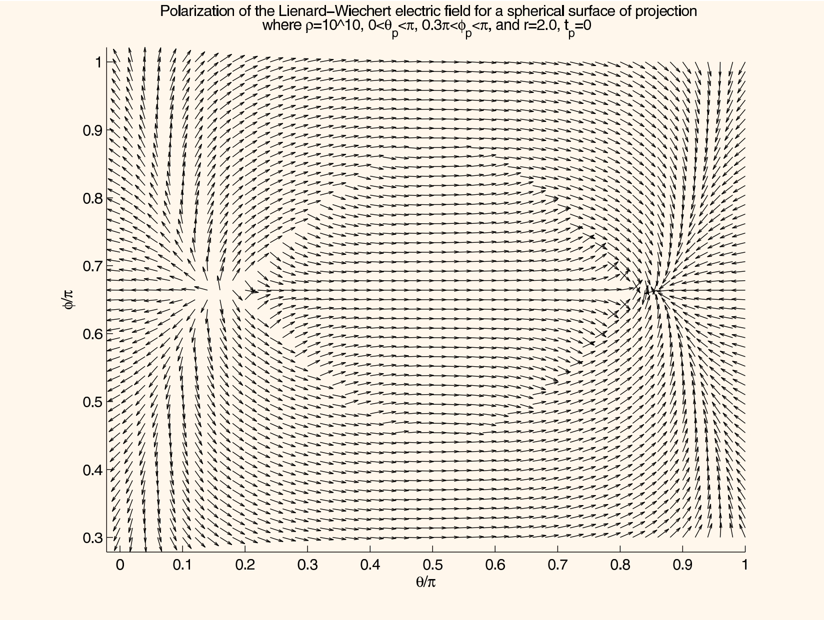

Figure 11: Polarization position angles of the total field on a sphere $R_P = 10^{10}c/\omega$, for $r\omega = 2c$. The longitude is plotted along the vertical axis in this figure and the arrows only indicate the direction and not the magnitude of the field. Note the 180° swings of the position angle in the vicinities of the two points at which the cusp intersects the sphere.

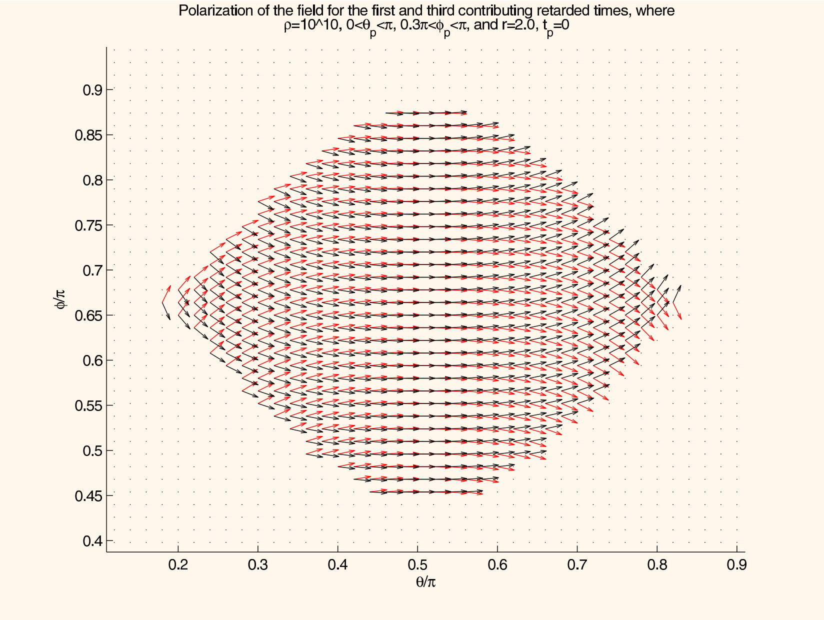

Figure 12: Polarization position angles of the two dominant polarization modes (inside the envelope) on a sphere $R_P = 10^{10}c/\omega$, for $r\omega = 2c$. The longitude is plotted along the vertical axis in this figure and the arrows only indicate the direction and not the magnitude of the field.